Materials Research. 2018; 21(2): e20170901
DOI: http://dx.doi.org/10.1590/1980-5373-MR-2017-0901

Microstructural evolution and mechanical properties of Sn-Bi-Cu ternary eutectic alloy produced by directional solidification

Mevlüt Şahin[a]*, Tolga Şensoy[b], Emin Çadırlı[c]

[a] *Niğde Ömer Halisdemir University, Technical Vocational School of Sciences, Department of Electronics and Automation, Niğde, Turkey*
[b] *Niğde Ömer Halisdemir University, Institute of Science and Technology, Department of Physics, Niğde, Turkey*
[c] *Niğde Ömer Halisdemir University, Faculty of Arts and Sciences, Department of Physics, Niğde, Turkey*

Received: October 03, 2017; Revised: December 13, 2017; Accepted: December 20, 2017

Sn-36Bi-22Cu (wt.%) ternary eutectic alloy was prepared using vacuum melting furnace and casting furnace. The samples were directionally solidified upwards solidification rate varying from 8.3 to 166 μm/s and at a constant temperature gradient (4.2 K/mm) in a Bridgman-type directional solidification furnace. The composition analysis of the phases and the intermetallics (Cu_3Sn and Cu_6Sn_5) were determined from EDX and XRD analysis respectively. The variation of the lamellar spacing (Bi-rich phase) and the Cu_3Sn phase spacing with the solidification rate were investigated. The dependence of microhardness, ultimate compressive strength and compressive yield strength on solidification rate were determined. The spacing and microhardness were measured from both longitudinal and transverse sections of the samples. The dependence of microhardness on the lamellar spacing and the Cu_3Sn phase spacing were also determined. The relationships between phase spacings, solidification rate and mechanical properties were determined from linear regression analysis.

Keywords: Directional solidification, eutectic alloy, microstructure, intermetallic compound, microhardness, compressive strength.

1. Introduction

Solidification plays a vital role since it forms the basis for influencing the microstructure and hence improving the quality of cast products. For this improving the casting production and solidification methods have a significant effect on the mechanical properties of the materials and enhancing the quality of cast metals[1-4]. Directional solidification[5] is one of the most important solidification methods used for material processing. The mechanical properties of the alloys can be improved by obtaining finer microstructure result from higher solidification rates and higher cooling rates under several directional solidification conditions[6-13]. The directionally solidified alloy exhibited higher strength than the non-directionally solidified alloy under the same cooling rate[14,15]. Liu et al.[16] reported that the tensile strength of the in situ composite from the directionally solidified alloy is significantly higher than that from the as-cast alloy.

Soldering technology is an essential part of electronic devices since it plays a key role not only as an electrical connection but also as a mechanical bond[17,18]. Currently, solder joints with higher reliability is demanding because the trend in electronic package is to make products smaller and faster. For global environment conservation, many researches on replacing the conventional Pb-Sn eutectic solder with a lead-free solder have been carried out. Among various lead-free solders, Sn-Bi alloy is one of the promising candidates[19]. Furthermore, the ternary Sn-Bi-Cu ternary alloys may also be considered as promising lead-free solders[19]. Recently, Ag, Bi or In-containing Sn-Cu alloys have received some attention, and in several prominent reliability test programs Sn-Cu-Ag and Sn-Cu-In alloys demonstrated superior performance, at least in its mechanical strength[20,21]. Tai et al.[22] showed that creep resistance of Sn-3.5Ag was improved significantly for Cu particle-reinforced composite solder joints at 25 °C, 65 °C and 105 °C. The tensile strength increased with increasing Bi content in the Sn-Cu eutectic solder alloy, which was attributed to the presence of Bi and its role in refining microstructure and solid solution strengthening[23]. Zhang et al.[24] reported that Sn-Bi-Cu alloys were found to have greater wettability than the Sn-Ag-Cu alloy, and it was confirmed that the addition of Bi increases the wettability. The effect of Cu_3Sn and Cu_6Sn_5 intermetallics (IMC's) on the mechanical properties were investigated from many researchers[25,26]. Cheng et al.[25] reported that, Cu_3Sn single crystal consist of high ultimate strengths depending on the material directions and strain rate. Hu et al.[26] reported that,

*e-mail: msahin@nigde.edu.tr

increased amount of Cu_6Sn_5 fibers caused an increment in both ultimate tensile strength and yield tensile strength. The mechanical properties (microhardness, shear stress, young and bulk modulus) and the wettability of the SnCu solder were improved with Bi addition[27]. There are numerous works on low solute content (Cu) Sn-based alloys[8,23-31]. Nevertheless, there has been only a limited amount of data about the mechanical properties of directionally solidified high solute content (Cu) Sn-based alloy. In this study, Sn-Bi-Cu ternary alloy containing high Cu is preferred. Similar alloys are used as soldering or brazing material depending on the content of copper. The aim of the present work is to investigate the effect of solidification rate (V) on microstructure (λ), microhardness (HV) and compressive strength (σ) of the directionally solidified Sn-36Bi-22Cu (wt.%) ternary eutectic alloy. The dependence of microhardness on the lamellar spacing (Bi-rich phase) and the Cu_3Sn IMC phase spacing were also determined.

2. Experimental Procedure

2.1. Alloy preparation, directional solidification and metallographic processes

Weighed quantities of Sn, Bi and Cu metals in a graphite crucible determined from stoichiometric calculations were placed in a vacuum melting furnace, and the metals were completely melted. After allowing time for the melt to become homogeneous, the molten alloy was poured into graphite crucibles in a casting furnace. The molten alloy solidified from bottom to top in the casting furnace. The directional solidification of the produced alloy was performed in a Bridgman-type directional solidification furnace whose schematic diagram is given in Figure 1. For the directional solidification, the sample was placed into the sample holder. The sample was placed into the furnace. After the furnace reached the desired temperature and thermal stabilization, the sample was withdrawn from the hot region to the cold region of the furnace with the help of different speeded synchronous motors. The alloy was directionally solidified under different solidification rates (8.3-166 μm/s) at a constant temperature gradient (4.2 K/mm). When the sample solidified 12-13 cm, it was quenched in water. Details of the furnaces equipment, alloy preparation, and directional solidification are given in previous work[32].

For the metallographic processes, the longitudinal and the transverse sections of the samples were cold mounted with epoxy-resin. The samples were then ground with 320-4000 grit SiC paper and polished with 3-0.25 μm diamond pastes. The alloys were then etched with 95 ml H_2O, 2.5 ml HNO_3, 1.5 ml HCI, 1 ml HF. The micrographs of the samples were taken with the Olympus BX-51 model optical microscope by using different objectives. The lamellar spacing, λ (Bi-rich phase) and the Cu_3Sn intermetallic phase spacings (λ_1) were measured with the Adobe Photoshop CS3 program taking into account the magnification factor. In eutectic and intermetallic phase spacing measurements, linear intersection method is used. In both measurements, at least 30-50 values were measured for each specimen at least on ten different regions for each specimen for statistical reliability. The details of eutectic and particle spacing measurements were described elsewhere[32].

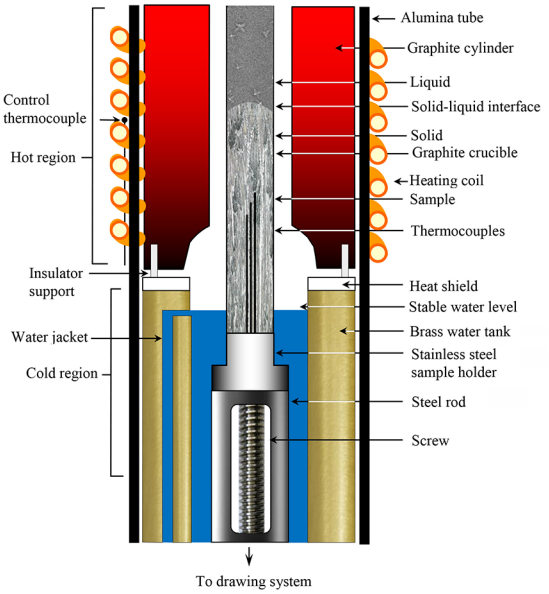

Figure 1. The Bridgman-type directional solidification furnace

2.2. Measurement of microhardness

Microhardness measurements were performed with a *Future Tech FM-700* model digital microhardness test device. This device has the ability of applying 1-1000 g load. In this work 10 g load was applied to the sample for 10 seconds. The measurements were taken from the solid parts nearest to the solid-liquid interface. Average of 30 measurements were taken from longitudinal and transverse sections of the directionally solidified samples, and the average values were taken for the microhardness value. When the indenter of the test device applied to the sample for certain times, the trace in the shape of square occurs. The diagonal size of the trace (d) is read from the test device. By dividing the applied force by the trace area the Vickers microhardness is determined as follows

$$HV = \frac{2P\sin(\theta/2)}{d^2} \quad (1)$$

where P is the applied load (kg), d is the diagonal length of trace, θ is the angle between the opposite surfaces of the diagonal trace.

2.3. Measurement of compressive strengths

The dependence of ultimate compressive strength and compressive yield strength on the solidification rate were determined. In this work, round rod samples have a length of 6-8 mm and a diameter of 4 mm were used. Compressive strength measurements of the samples were made at room temperature at a deformation rate of 1 mm/min. Compressive tests were performed to the directionally solidified round rod samples with different solidification rates.

3. Results and Discussion

3.1 Determination of the chemical components of the phases

According to the binary phase diagrams among Bi, Sn and Cu, solid solubility of Sn in solid Bi and Bi in solid Sn are about 0.1 wt.% Sn and 21 wt.% Bi, respectively at the eutectic temperature, 139°C[33]. Also, the solubility of solid Sn in Cu and solid Cu in Sn are about 1 wt.% and 0.006 wt.%, respectively at the eutectic temperature, 232°C[33]. Previous work[34] indicated that the calculated solubilities of Bi in solid Cu or Cu in solid Bi at the eutectic point are both approximately 10^{-9} with the assumption that the interchange energy in the rhombohedral structure is similar to that in the fcc structure. This small amount cannot be detected with modern spectroscopy, and the material is normally treated as a pure material[34].

Energy dispersive X-ray (EDX) analysis was performed to determine the composition of phases in the Sn-Bi-Cu eutectic alloy. EDX analysis was performed at 20 keV using the X-ray lines. According to the EDX analysis results shown in Figure 2, four different solid phases (black, dark gray, white lamellar and dark lamellar) grew at the Sn-Bi-Cu eutectic alloy. The compositions of the black phase (Cu_3Sn intermetallic) and dark gray phase (Cu_6Sn_5 intermetallic) were Cu-wt.% 40.70 Sn and Sn-wt.% 35.75 Cu, respectively. Also, the white lamellar phase (Bi-rich eutectic) and dark lamellar phase (Sn-rich eutectic) were Bi-3.38 wt.% Sn and Bi-24.16 wt.% Sn, respectively. Figure 2 shows examples of representative SEM images of ternary eutectic microstructures obtained for the directionally solidified Sn-36Bi-22Cu alloys, with the eutectic mixtures being characterized by complex arrangements of Bi-rich and Sn-rich phases and the corresponding intermetallic compounds, Cu_3Sn and Cu_6Sn_5, respectively. For the Cu_3Sn IMC, its growth is governed by the reaction between Cu and Sn atoms. Clevenger et al.[35] reported the onset of Cu_3Sn formation from the reaction between Cu_6Sn_5 and Cu. The Cu_3Sn phase can be formed by conventional casting[36,37], directional solidification[8,23,26] and rapid solidification methods[38-40]. Due to the solidification temperature differences, initially the Cu-rich Cu_3Sn and Cu_6Sn_5 IMC phases solidified, followed by Sn-rich and Bi-rich phases at a lower temperature. Ternary cooperative growth has not been observed for this reason. In addition, the presence of these phases was confirmed by EDX (Fig.2) and XRD analysis (Fig.3). According to Fig.2, Cu_3Sn particles with a thickness about 4 μm were surrounded by Cu_6Sn_5 phase and these two phases are coherent with each other very well. During the eutectic reaction, the Cu_3Sn IMC phase grows as rods embedded in a continuous Bi-rich matrix.

X-ray diffraction (XRD) measurements were performed with a diffractometer (Rigaku Ultima IV) using Cu-Kα radiation (k=1.5405 A°) at an accelerating voltage of 40 kV. The diffracted beam was scanned in steps by 0.01º across a 2θ range of 10-100º. XRD results of as-cast alloy are shown in Figure 3. As indicated, the presence of Cu_3Sn and Cu_6Sn_5 is confirmed due to the high number of peaks corresponding to these phases. Bi was not observed present in the Cu_3Sn and Cu_6Sn_5 IMC phases, and Bi did not form IMCs in the interfacial reactions. The Cu_3Sn and Cu_6Sn_5 intermetallics have rod-like morphologies, being characterized as faceted phases. Cu_3Sn IMC is a more stable phase than Cu_6Sn_5 IMC. The Cu_3Sn intermetallic particles may grow in a rod-like form without branches, as shown in Figure 4. Kim et al.[41] reported similar morphologies for the Cu_6Sn_5 and Ag_3Sn particles in Sn-Ag-Cu alloys.

3. 2 Effect of solidification rate on microstructure

The optic micrographs of the longitudinal and transverse sections of directionally solidified Sn-Bi-Cu eutectic alloy at different solidification parameters are shown in Figure 4. The microstructure is formed by dispersed rod-like particles of Cu_3Sn within Sn-rich and Bi-rich phases. Cu_3Sn IMC appears for each solidification rate. Cooling condition has a significant effect on the IMC thickness. For a constant temperature gradient (4.2 K/mm), it is found that the complex regular Bi-Sn lamellar spacings and Cu_3Sn intermetallic phase spacings are mainly controlled by the solidification rate (V), and both of them decrease with increased solidification rate. Spacings between primary intermetallic particles (Cu_3Sn) were measured. These particles are part of the complex regular eutectic microstructure. At the highest growth rate (166 μm/s), the average spacing between the particles is reduced to 22 μm. Consequently, the microstructure underwent are finement with an increase in the solidification rate (Table 1).

Higher solidification rate yields a thinner IMC, which is consistent with other researchers' results[42,43]. Because of its mechanical properties, Cu_3Sn is also more suitable than Cu_6Sn_5 and Sn as a joint material for microbumps[44,45].

Rod-like Cu_3Sn particles prevailed along the Bi-rich eutectic matrix, as can be seen in Fig. 4. These hard and brittle Cu_3Sn particles are normally alternated with the Bi-rich phase permitting the eutectic mixture to be characterized. According to Figure 4, The primary Cu_3Sn intermetallic phases with a thickness about 4 μm were surrounded by Cu_6Sn_5 intermetallic phases for lowest solidification rate (8.3 μm/s) and these two

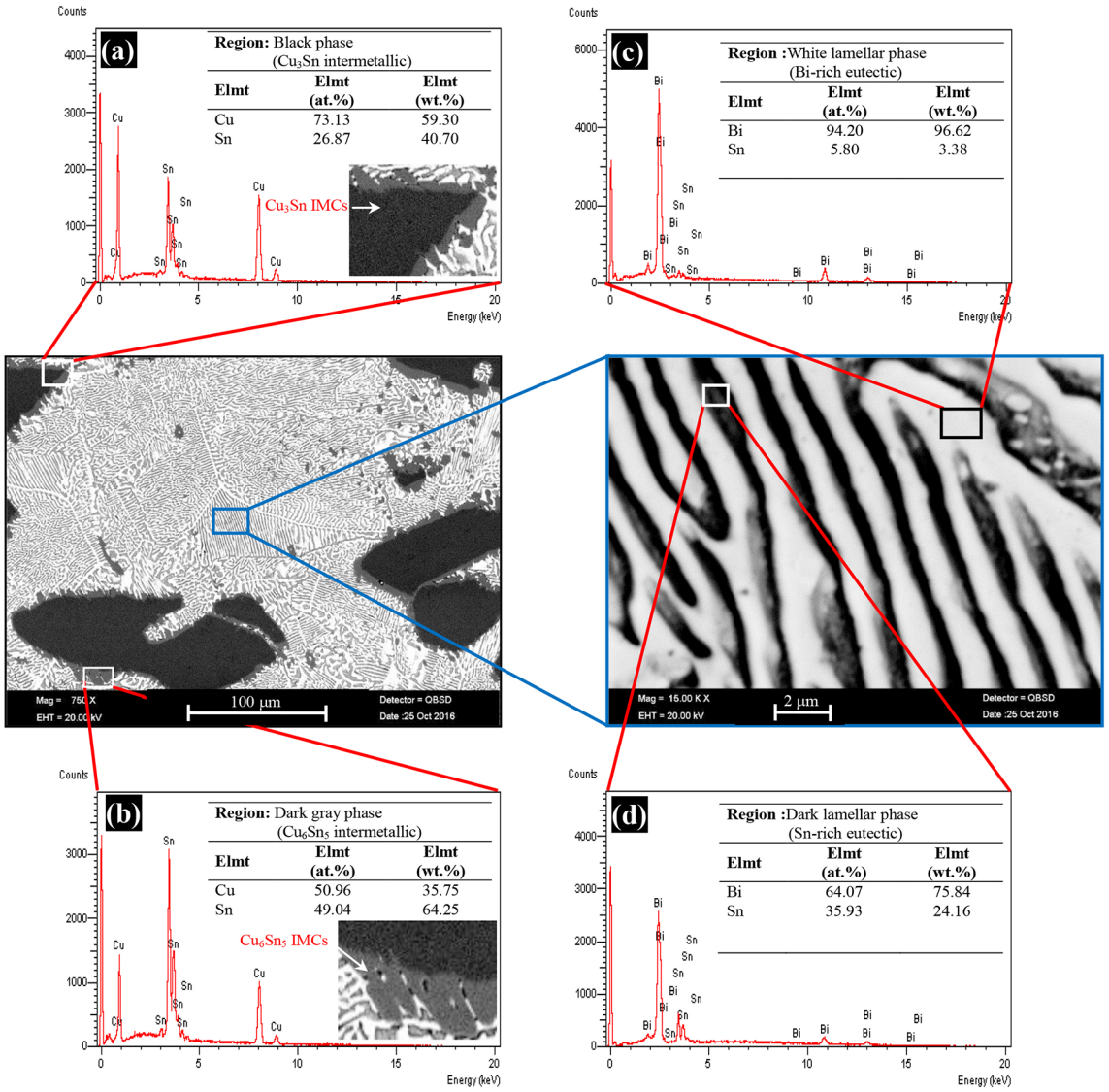

Figure 2. The chemical composition analysis of Sn-36Bi-22Cu eutectic alloy (G=4.2 K/mm, V=8.3 µm/s) by using SEM-EDX, (a) black phase (Cu_3Sn intermetallic phase) (b) dark gray phase (Cu_6Sn_5 intermetallic phase) (c) white lamellar phase (Bi-rich eutectic phase) (d) dark lamellar phase (Sn-rich eutectic phase)

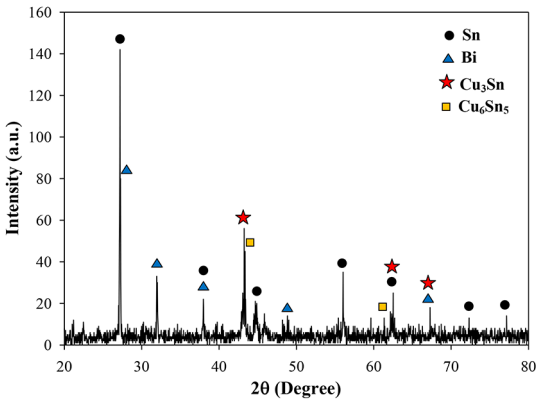

Figure 3. X-ray diffraction patterns obtained from the Sn-36Bi-22Cu alloy

phases are coherent with each other very well. With increasing the solidification rate from 8.3 to 166 µm/s, the thickness of Cu_6Sn_5 intermetallic phase decreased from 4.15 µm to 0.75 µm. The thickness of the Cu_6Sn_5 phase agrees with the thickness found by Chen[46], Le et al.[47] and Rao et al.[48]. The variation of lamellar spacing (λ) and Cu_3Sn intermetallic phase spacing (λ_I) with solidification rate are given in Table 1 and Figure 5, and the relationships between these parameters are given in Table 2. At a constant temperature gradient (4.2 K/mm), the λ and λ_I decreased with increasing solidification rate. The average eutectic spacing values measured on the longitudinal (λ_L) and transverse (λ_T) sections of the samples are given in Table 1. With increasing the solidification rate from 8.3 to 166 µm/s, λ_L (lamellar) decreased from 2.72 to

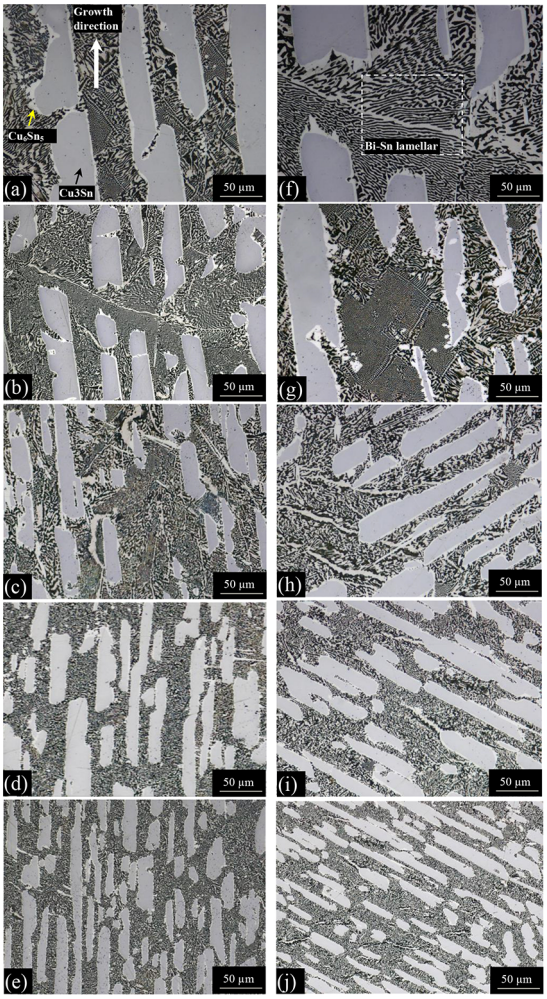

Figure 4. Optical images of the directionally solidified Sn-36Bi-22Cu eutectic alloy at a constant temperature gradient (G=4.2 K/mm) (a-e) longitudinal section (V=8.3-166.0 µm/s), (f-j) transverse section (V=8.3-166.0 µm/s)

1.41 µm, λ_T (lamellar) decreased from 2.89 to 1.50 µm, λ_{IL} (for Cu_3Sn phase) decreased from 98.3 to 18.6 µm and λ_{IT} (for Cu_3Sn phase) decreased from 108.0 to 25.4 µm. The exponent value (0.24-0.25) of the V is in good agreement with the values of 0.22-0.26, 0.25 obtained by Şahin and Çadırlı[49] for Bi-2.0Zn-0.2Al (wt.%) eutectic alloy, by Yan et al.[50] for Nb-22Ti-16Si-3Cr-3Al-2Hf (at.%) alloy, respectively. Since ternary cooperative growth has not been observed in this study, the exponent value of 0.5 predicted by the Jackson-Hunt eutectic theory[51] for binary eutectics was not obtained. However, as can be seen from Table 2, an exponent value of 0.52 was obtained for the dependence of the Cu_3Sn phase spacings related to solidification rate.

3.3. Effect of solidification rate on microhardness

The dependence of microhardness on the solidification rate and phase spacing is given in Table 1 and Figures 6 and 7, and the relationships between these parameters are given in Table 3. At a constant temperature gradient (4.2 K/mm), the microhardness values increased with increasing solidification rate. The average microhardness values measured on the longitudinal and transverse sections of the samples are given in Table 1. With increasing the solidification rate from 8.3 to 166 µm/s, the HV_L increased from 192.7 to 290.8 MPa and HV_T increased from 193.2 to 296.7 MPa. Also, the HV_{IL} (Cu_3Sn phase) increased from 3054.8 to 3436.4 MPa and HV_{IT} (Cu_3Sn phase) increased from 2663.4 to 3144.1 MPa. The measured microhardness values for the Cu_3Sn phase are in good agreement with the values of 3364.8, 3266.7-2795.9 (0.98-4.9 N load), 3364.8 and lower than the 4231.1-4184.9 MPa (1.96-4.9 N load) obtained by Lee et al.[52], Liu et al.[53], Frear et al.[54] and Ghosh[55], respectively.

The exponent value (0.13-0.14) of the V (for lamellar structure) is in good agreement with the value of 0.14, 0.11, 0.15, values obtained by Zhang et al.[7] for Ni-25at.%Si alloy, by Hu et al.[56] for Sn-1.0 wt.% Cu, by Fan et al.[57] for Ti-46Al-0.5W-0.5Si alloy (at.%), respectively. Decrease in lamellar spacing due to the increasing solidification rate, increased the microhardness. As can be seen from Table 1 and Figure 7, microhardness increased with decreasing lamellar spacing. With decreasing the λ_L from 2.72 to 1.41 µm, HV_L increased from 192.7 to 290.8 MPa. With decreasing the λ_{IL} from 98.3 to 18.6 µm, HV_{IL} increased from 3054.8 to 3436.4 MPa. Similarly, With decreasing the λ_T from 2.89 to 1.50 µm, HV_T increased from 193.2 to 296.7 MPa. With decreasing the λ_{IT} from 108.0 to 25.4 µm, HV_{IT} increased from 2663.4 to 3144.1 MPa.

The increment of the solidification rate not only decrease the Cu_3Sn IMC spacings but also refines the Cu_3Sn IMC phases. The finer microstructure causes an increment on the mechanical properties. The microhardness values of the Cu_3Sn phases are approximately 10-15 times greater than the complex Bi-Sn eutectic phase. However, the change in complex lamellar spacing is more effective on microhardness. As shown in Table 3, the exponent value (0.53) of the Bi-Sn complex lamellar phase is quite larger than the exponent value (0.09) of the Cu_3Sn IMC phase. This is due to the fact that the dependency of the Bi-Sn complex lamellar spacing on the solidification rate is quite large relative to the Cu_3Sn IMC phase spacing. The exponent value (0.53) of the lamellar phase is good agreement with the 0.50 value obtained by Spinelli et al.[30] for Sn-Cu solder alloys

Table 1. Experimental data of the Sn-36Bi-22Cu alloy.

G (K/mm)	V (μm/s)	λ (μm)	λ_I (μm)	HV (MPa)	Thickness of Cu_6Sn_5 (μm)	HV_I (MPa)	σ_y (MPa)	σ_c (MPa)
4.2	8.3	2.81	103.1	192.9	4.15	2859.1	71.5	102.1
4.2	16.6	2.60	73.2	215.1	3.29	2958.2	91.0	110.0
4.2	41.5	1.78	37.2	233.6	2.10	3042.1	103.3	113.0
4.2	83.0	1.51	30.4	260.0	1.68	3124.5	112.3	116.3
4.2	166.0	1.46	22.0	293.7	0.75	3290.3	118.9	139.3

λ: the value of the lamellar spacing
λ_I: the value of the Cu_3Sn intermetallic phase spacing
HV: the microhardness value of the lamellar structure
HV_I:the microhardness value of the Cu_3Sn intermetallic phase
σ_y: the value of the compressive yield strength
σ_c: the value of the ultimate compressive strength.

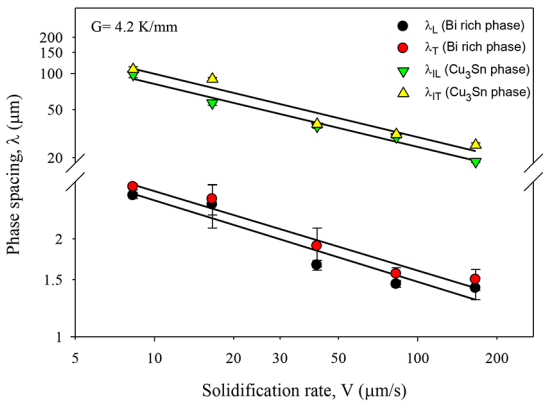

Figure 5. Variation of phase spacings versus solidification rate

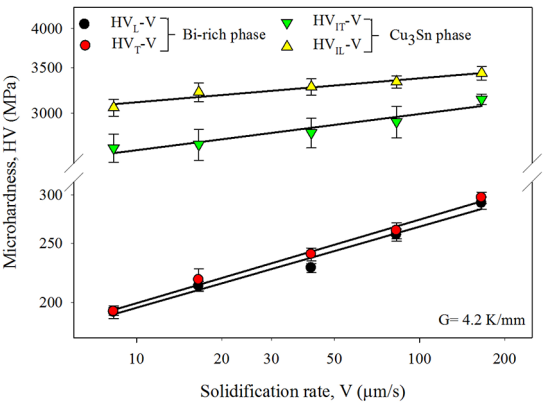

Figure 6. Variation of microhardness versus solidification rate

Table 2. The relationships between the microstructure parameters and the solidification rate

Relationships	Constant (k)	Correlation Coefficient (r)
$\lambda_{IL}=k_1V^{-0.52}$	k_1=273.53 ($\mu m^{1.52}s^{-0.52}$)	r_1= -0.990
$\lambda_{IT}=k_2V^{-0.53}$	k_2=333.43 ($\mu m^{1.53}s^{-0.53}$)	r_2= -0.973
$\lambda_L=k_3V^{-0.25}$	k_3=4.68 ($\mu m^{1.25}s^{-0.25}$)	r_3= -0.960
$\lambda_T=k_4V^{-0.24}$	k_4=4.92 ($\mu m^{1.24}s^{-0.24}$)	r_4= -0.979

λ_{IL}: the spacings between the Cu_3Sn intermetallic phases measured from the longitudinal section of the sample
λ_{IT}: the spacings between the Cu_3Sn intermetallic phases measured from the transverse section of the sample
λ_L: the values of the lamellar spacing (Bi rich phase) measured from the longitudinal section of the sample
λ_T: the values of the lamellar spacing (Bi rich phase) measured from the transverse section of the sample.

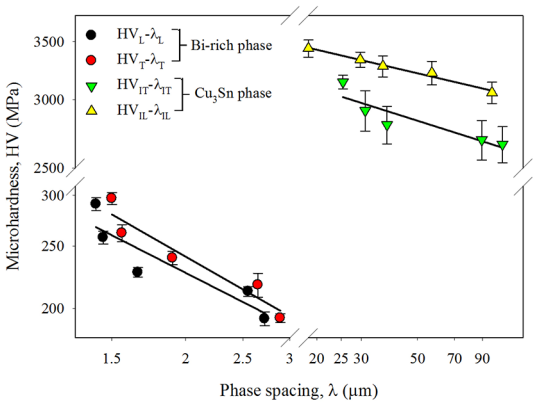

Figure 7. Variation of microhardness versus phase spacing

Table 3. The relationships between the solidification rate and the mechanical properties

Relationships	Constant (k)	Correlation Coefficient (r)
$HV_L=k_1V^{0.13}$	k_1=360.83 (MPa $mm^{-0.13}s^{0.13}$)	r_1= 0.989
$HV_T=k_2V^{0.14}$	k_2=374.11 (MPa $mm^{-0.14}s^{0.14}$)	r_2= 0.996
$HV_{IL}=k_3V^{0.04}$	k_3=3660.16 (MPa $mm^{-0.04}s^{0.04}$)	r_3= 0.971
$HV_{IT}=k_4V^{0.05}$	k_4=3379.87 (MPa $mm^{-0.05}s^{0.05}$)	r_4= 0.959
$HV_L=k_5\lambda^{-0.47}$	k_5=12.31 (MPa $mm^{0.47}$)	r_5= -0.913
$HV_T=k_6\lambda^{-0.53}$	k_6=9.15 (MPa $mm^{0.53}$)	r_6= -0.956
$HV_{IL}=k_7\lambda^{-0.07}$	k_7=2622.41 (MPa $mm^{0.07}$)	r_7= -0.991
$HV_{IT}=k_8\lambda^{-0.09}$	k_8=2145.85 (MPa $mm^{0.09}$)	r_8= -0.902
$\sigma_c=k_9V^{0.09}$	k_9=153.74 (MPa $mm^{-0.09}s^{0.09}$)	r_9= 0.914
$\sigma_y=k_{10}V^{0.16}$	k_{10}=165.99 (MPa $mm^{-0.16}s^{0.16}$)	r_{10}= 0.962

HV_L: the value of the microhardness measured from the longitudinal section of the lamellar structure
HV_T: the value of the microhardness measured from the transverse section of the lamellar structure
HV_{IL}: the value of the microhardness measured from the longitudinal section of the Cu_3Sn intermetallic phase
HV_{IT}: the value of the microhardness measured from the transverse section of the Cu_3Sn intermetallic phase
σ_c: the values of the ultimate compressive strength
σ_y: the values of the compressive yield strength

3.4 Effect of solidification rate on compressive strength

Compressive strength-strain curves for Sn-36Bi-22Cu alloy are shown in Figure 8. The variation of ultimate compressive strength (σ_c) and compressive yield strength (σ_y) determined form strength-strain curves with solidification rate are given in Figure 9 and Table 1, and the relationships between these parameters are given in Table 3. At a constant temperature gradient (4.2 K/mm), the compressive strength values increased with increasing solidification rate. With increasing the solidification rate from 8.3 to 166 µm/s, the σ_c increased from 102.1 to 139.3 MPa and the σ_y increased from 71.5 to 118.9 MPa. The exponent value (0.09) of the V for the σ_c is in good agreement with the 0.08, 0.08, 0.11 values of σ_t obtained by Hu et al.[23] for Sn-0.7Cu-0.7Bi (wt.%) alloy, by Hosch and Napolitano[58] for Al-12wt.%Si alloy, by Çadırlı et al.[59] for Sn-40.5Pb-2.6Sb (wt.%) ternary eutectic alloy respectively. The exponent value (0.16) of the V for the σ_c is in good agreement with the 0.16 value of the σ_t obtained by Hu et al.[23] for Sn-0.7Cu-0.7Bi (wt.%) alloy.

Nevertheless, the exponent value (0.09) of the V for the ultimate compressive strength is higher than the 0.04 value of ultimate tensile strength and the exponent value (0.16) of the V for the compressive yield strength is slightly higher than the 0.12 value of the tensile yield strength, σ, obtained by Hu et al.[23] for Sn-0.7Cu-1.3Bi (wt.%) alloy. Differences exist in the exponent values because of the possible differences in purity, different alloy compositions, solidification conditions and the surface preparation of the test pieces. Also, solidification rate effects the elongation of the alloy. Hu et al.[26] determined that, with increasing solidification rate from 5 to 100 µm/s, the elongation increased from % 28.2 to % 41.5 for Sn-0.7Cu-0.7Bi (wt.%) alloy. Sakuyama et al.[36] found that, the elongation of the Bi-41.8Sn-0.5Cu is higher than the Bi-41.8Sn-0.5Ag, Bi-41.8Sn-0.5Zn and Bi-42Sn alloys. This situations improve the importance of the material for technological applications.

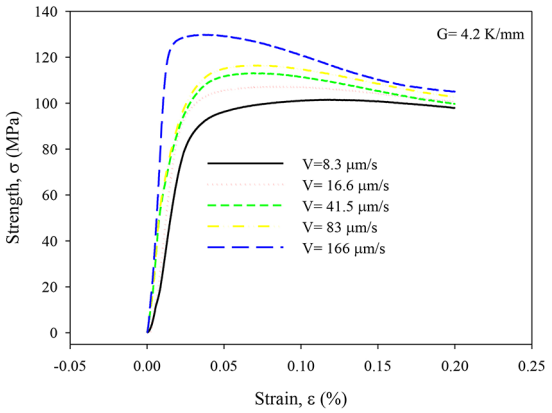

Figure 8. Typical strength-strain curves of Sn-36Bi-22Cu eutectic alloy for different V at a constant G

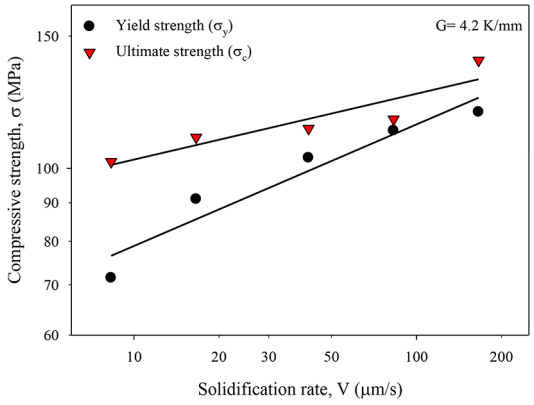

Figure 9. Variation of compressive strength of the Sn-36Bi-22Cu alloy as a function of solidification rate

According to the literature[60], it is well established that the two IMCs are the ε-phase (Cu_3Sn) and η-phase (Cu_6Sn_5). The presence of those intermetallic phases may increase HV and σ, but the ductility properties slightly decrease with further increased solidification rate, that may contribute to a reason. The main reason is that the high growth velocity during directional solidification may result in a radial temperature gradient, which leads to some Cu_3Sn fibers do not grow along with the crystal growth direction. Consequently, the increment in the solidification rate caused finer microstructure. This finer microstructure has improved the some mechanical properties (HV, σ_c) of the Sn-Bi-Cu ternary eutectic alloy. The crucial role in this solidification process was played

by Cu_3Sn and Cu_6Sn_5 IMCs in the Sn-matrix of Sn-Bi-Cu ternary system. These IMC phases build a long-range internal stress, resulting in a strengthening effect.

4. Conclusions

Sn-36Bi-22Cu (wt.%) ternary eutectic alloy was directionally solidified upwards at a constant temperature gradient (4.2 K/mm) under different solidification rates (8.3-166μm/s) in a Bridgman-type directional solidification furnace. The results are summarized as follows:

1. The lamellar spacing and the Cu_3Sn phase spacing decreased with increasing solidification rate. With increasing the solidification rate from 8.3 to 166 μm/s, average λ decreased from 2.81 to 1.46 μm, average λ_I decreased from 103.1 to 22.0 μm for the lamellar spacing and Cu_3Sn phase spacing, respectively. The relationships between the eutectic spacings and solidification rate were obtained by binary regression analysis as ($\lambda_L=4.7V^{-0.25}$,$\lambda_{IL}=273V^{-0.52}$)
2. The microhardness increased with increasing solidification rate. Average HV increased from 192.9 to 293.7 MPa, and HV_I increased from 2859.1 to 3290.3 MPa with increasing the solidification rate from 8.3 to 166 μm/s. The establishment of the relationship between *HV* and *V* can be given as ($HV=367.3V^{0.13}$,$HV=3520.5V^{0.04}$)
3. The compressive strength values increased with increasing solidification rate. The σ_c increased from 102.1 to 139.3 MPa and the σ_y increased from 71.5 to 118.9 MPa with increasing the solidification rate from 8.3 to 166 μm/s. The relationships between σ and *V* can be given as ($\sigma_c=153V^{0.09}$,$\sigma_y=165V^{0.16}$).

5. References

1. Stefanescu DM. *Science and Engineering of Casting Solidification*, Kluwer Academic/Plenum Publishers, New York, 2002.
2. Campbell J. Effects of vibration during solidification. *International Metals Reviews*. 1981;26(1):71-108.
3. Verma A, Tewari SP, Prakash J. Vibratory stress, solidification and microstructure of weldments under vibratory welding condition - A review. *International Journal of Engineering Science and Technology*. 2011;3(6):5215-5220.
4. Yao L, Hao H, Ji SH, Fang CF, Zhang XG. Effects of ultrasonic vibration on solidification structure and properties of Mg-8Li-3Al alloy. *Transactions of Nonferrous Metals Society of China*. 2011;21(6):1241-1246.
5. Gündüz M, Çadırlı E. Directional solidification of aluminium-copper alloys. *Materials Science and Engineering: A*. 2002;327(2):167-185.
6. Verissimo NC, Brito C, Santos WLR, Cheung N, Spinelli JE, Garcia A. Interconnection of Zn content, macrosegregation, dendritic growth, nature of intermetallics and hardness in directionally solidified Mg-Zn alloys. *Journal of Alloys and Compounds*. 2016;662:1-10.
7. Zhang B, Li X, Wang T, Liu Z. Microstructures and mechanical properties of directionally solidified Ni-25%Si full lamellar in situ composites. *Materials Science and Engineering: A*. 2016;674:242-249.
8. Silva BL, Garcia A, Spinelli JE. Complex eutectic growth and Bi precipitation in ternary Sn-Bi-Cu and Sn-Bi-Ag alloys. *Journal of Alloys and Compounds*. 2017;691:600-605.
9. Luo S, Yang G, Liu S, Wang J, Li J, Jie W. Microstructure evolution and mechanical properties of directionally solidified Mg-xGd (x=0.8, 1.5, and 2.5) alloys. *Materials Science and Engineering: A*. 2016;662:241-250.
10. Reyes RV, Bello TS, Kakitani R, Costa TA, Garcia A, Cheung N, et al. Tensile properties and related microstructural aspects of hypereutectic Al-Si alloys directionally solidified under different melt superheats and transient heat flow conditions. *Materials Science and Engineering: A*. 2017;685:235-243.
11. Fan J, Liu J, Tian S, Wu S, Wang S, Gao H, et al. Effect of solidification parameters on microstructural characteristics and mechanical properties of directionally solidified binary TiAl alloy. *Journal of Alloys and Compounds*. 2015;650:8-14.
12. Bertelli F, Freitas ES, Cheung N, Arenas MA, Conde A, Damborenea J, et al. Microstructure, tensile properties and wear resistance correlations on directionally solidified Al-Sn-(Cu; Si) alloys. *Journal of Alloys and Compounds*. 2017;695:3621-3631.
13. Zhai W, Wang B, Hu L, Wei B. Ternary eutectic growth during directional solidification of Ag-Cu-Sb alloy. *Philosophical Magazine Letters*. 2015;95(4):187-193.
14. Liu S, Yang G, Jie W. Microstructure, Microsegregation, and Mechanical Properties of Directional Solidified Mg-3.0Nd-1.5Gd Alloy. *Acta Metallurgica Sinica (English Letters)*. 2014;27(6):1134-1143.
15. Wang JH, Yang GY, Liu SJ, Jie WQ. Microstructure and room temperature mechanical properties of directionally solidified Mg-2.35Gd magnesium alloy. *Transactions of Nonferrous Metals Society of China*. 2016;26(5):1294-1300.
16. Liu K, Jiang Z, Zhao J, Zou J, Chen Z, Lu D. Effect of directional solidification rate on the microstructure and properties of deformation-processed Cu-7Cr-0.1Ag in situ composites. *Journal of Alloys and Compounds*. 2014;612:221-226.
17. Kang SK, Sarkhel AK. Lead (Pb)-free solders for electronic packaging. *Journal of Electronic Materials*. 1994;23(8):701-707.
18. Liu KC, Duh JG. Microstructural evolution in Sn/Pb solder and Pd/Ag thick film conductor metallization. *IEEE Transactions on Components, Hybrids, and Manufacturing Technology*. 1991;14(4):703-707.
19. Lee JI, Chen SW, Chang HY, Chen CM. Reactive wetting between molten Sn-Bi and Ni substrate. *Journal of Electronic Materials*. 2003;32(3):117-122.
20. El-Daly AA, Hammad AE. Development of high strength Sn-0.7Cu solders with the addition of small amount of Ag and In. *Journal of Alloys and Compounds*. 2011;509(34):8554-8560.

21. El-Daly AA, Hammad AE. Enhancement of creep resistance and thermal behavior of eutectic Sn-Cu lead-free solder alloy by Ag and In-additions. *Materials & Design*. 2012;40:292-298.

22. Tai F, Guo F, Han MT, Xia ZD, Lei YP, Shi YW. Creep and thermomechanical fatigue properties of in situ Cu_6Sn_5 reinforced lead-free composite solder. *Materials Science and Engineering: A*. 2010;527(15):3335-3342.

23. Hu X, Li Y, Liu Y, Min Z. Developments of high strength Bi-containing Sn0.7Cu lead-free solder alloys prepared by directional solidification. *Journal of Alloys and Compounds*. 2015;625:241-250.

24. Zhang X, Matsuura H, Tsukihashi F, Yuan Z. Wettability of Sn-Zn, Sn-Ag-Cu and Sn-Bi-Cu alloys on copper subsrates. *Materials Transactions*. 2012;53(5):926-931.

25. Cheng HC, Yu CF, Chen WH. Strain- and strain-rate-dependent mechanical properties and behaviors of Cu_3Sn compound using molecular dynamics simulation. *Journal of Materials Science*. 2012;47(7):3103-3114.

26. Hu X, Li K, Min Z. Microstructure evolution and mechanical properties of Sn0.7Cu0.7Bi lead-free solders produced by directional solidification. *Journal of Alloys and Compounds*. 2013;566:239-245.

27. Mohammed S, El-Maghraby A. Study of some mechanical properties and wetting behavior with addition Bi to SnCu solder alloys. *International Journal of Innovative Research in Science, Engineering and Technology*. 2014;3(2):9439-9446.

28. Silva BL, Garcia A, Spinelli JE. Cooling thermal parameters and microstructure features of directionally solidified ternary Sn-Bi-(Cu,Ag) solder alloys. *Materials Characterization*. 2016;114:30-42.

29. Yang TL, Wu JY, Li CC, Yang S, Kao CR. Low temperature bonding for high temperature applications by using SnBi solders. *Journal of Alloys and Compounds*. 2015;647:681-685.

30. Spinelli JE, Garcia A. Microstructural development and mechanical properties of hypereutectic Sn-Cu solder alloys. *Materials Science and Engineering: A*. 2013;568:195-201.

31. Wang KK, Gan D, Hsieh KC. The orientation relationships of the Cu3Sn/Cu interfaces and a discussion of the formation sequence of Cu_3Sn and Cu_6Sn_5. *Thin Solid Films*. 2014;562:398-404.

32. Sahin M. *The directional solidification of binary and ternary metallic alloys and investigation the physical properties of them*. [Thesis]. Nigde: Nigde University; 2012.

33. Hansen M, Anderko K. *Constitutions of Binary Alloys*. New York: McGraw-Hill; 1958.

34. Chang LS, Straumal BB, Rabkin E, Gust W, Sommer F. The Solidus Line of the Cu-Bi Phase Diagram. *Journal of Phase Equilibria*. 1997;18(2):128-135.

35. Clevenger LA, Arcot B, Ziegler W, Colgan EG, Hong QZ, d'Heurle FM, et al. Interdiffusion and phase formation in Cu(Sn) alloy films. *Journal of Applied Physics*. 1998;83(1):90-99.

36. Sakuyama S, Akamatsu T, Uenishi K, Sato T. Effects of a Third Element on Microstructure and Mechanical Properties of Eutectic Sn-Bi Solder. *Transactions of The Japan Institute of Electronics Packaging*. 2009;2(1):98-103.

37. Wang KK, Gan D, Hsieh KC. The orientation relationships of the Cu3Sn/Cu interfaces and a discussion of the formation sequence of Cu3Sn and Cu6Sn5. *Thin Solid Films*. 2014;562:398-404.

38. Shen J, Liu YC, Gao HX. Formation of bulk Cu_6Sn_5 intermetallic compounds in Sn-Cu lead-free solders during solidification. *Journal of Materials Science*. 2007;42(14):5375-5380.

39. El Ashram T, Shalaby RM. Effect of rapid solidification and small additions of Zn and Bi on the structure and properties of Sn-Cu eutectic alloy. *Journal of Electronic Materials*. 2005;34(2):212-215.

40. Zhai W, Wang BJ, Lu XY, Wei B. Rapid solidification mechanism of highly undercooled ternary $Cu_{40}Sn_{45}Sb_{15}$ alloy. *Applied Physics A*. 2015;121(1):273-281.

41. Kim KS, Huh SH, Suganuma K. Effects of intermetallic compounds on properties of Sn-Ag-Cu lead-free soldered joints. *Journal of Alloys and Compounds*. 2003;352(1-2):226-236.

42. Ochoa F, Williams JJ, Chawla N. Effects of cooling rate on the microstructure and tensile behavior of a Sn-3.5wt.%Ag solder. *Journal of Electronic Materials*. 2003;32(12):1414-1420.

43. Deng X, Piotrowski G, Williams JJ, Chawla N. Influence of initial morphology and thickness of $Cu_6Sn_5$and Cu_3Sn intermetallics on growth and evolution during thermal aging of Sn-Ag solder/Cu joints. *Journal of Electronic Materials*. 2003;32(12):1403-1413.

44. Bosco NS, Zok FW. Critical interlayer thickness for transient liquid phase bonding in the Cu-Sn system. *Acta Materialia*. 2004;52(10):2965-2972.

45. Deng X, Chawla N, Chawla KK, Koopman M. Deformation behavior of (Cu, Ag)-Sn intermetallics by nanoindentation. *Acta Materialia*. 2004;52(14):4291-4303.

46. Chen Z. *Micro-mechanical characteristics and dimensional change of Cu-Sn interconnects due to growth of interfacial intermetallic compounds*. [Thesis]. Loughborough: Loughborough University; 2014.

47. Lee HT, Chen MH, Jao HM, Liao TL. Influence of interfacial intermetallic compound on fracture behavior of solder joints. *Materials Science and Engineering: A*. 2003;358(1-2):134-141.

48. Chandra Rao BSS, Weng J, Shen L, Lee TK, Zeng KY. Morphology and mechanical properties of intermetallic compounds in SnAgCu solder joints. *Microelectronic Engineering*. 2010;87(11):2416-2422.

49. Şahin M, Çadırlı E. Mechanical, electrical, and thermal properties of the directionally solidified Bi-Zn-Al ternary eutectic alloy. *International Journal of Minerals, Metallurgy, and Materials*. 2014;21(10):999-1008.

50. Yan Y, Ding H, Kang Y, Song J. Microstructure evolution and mechanical properties of Nb-Si based alloy processed by electromagnetic cold crucible directional solidification. *Materials & Design*. 2014;55:450-455.

51. Jackson KA, Hunt JD. Lamellar and rod eutectic growth. *Transactions of the Metallurgical Society of AIME*. 1966;236:1129-1142.

52. Lee CC, Wang PJ, Kim JS. Are Intermetallics in Solder Joints Really Brittle? In: *Proceedings of the 57th Electronic Components and Technology Conference*; 2007 May 29-Jun 1; Reno, NV, USA.

53. Liu CY, Hu YJ, Liu YS, Tseng HW, Huang TS, Lu CT, et al. Epitaxial Cu-Sn bulk crystals grown by electric current. *Acta Materialia*. 2013;61(15):5713-5719.

54. Frear DR, Burchett SN, Morgan HS, Lau JH. *The Mechanics of Solder Alloy Interconnects*. New York: Van Nostrand Reinhold; 1994.

55. Ghosh G. Elastic properties, hardness, and indentation fracture toughness of intermetallics relevant to electronic packaging. *Journal of Materials Research*. 2004;19(5):1439-1454.

56. Hu X, Chen W, Wu B. Microstructure and tensile properties of Sn-1Cu lead-free solder alloy produced by directional solidification. *Materials Science and Engineering: A*. 2012;556:816-823.

57. Fan J, Li X, Su Y, Guo J, Fu H. Dependency of microhardness on solidification processing parameters and microstructure characteristics in the directionally solidified Ti-46Al-0.5W-0.5Si alloy. *Journal of Alloys and Compounds*. 2010;504(1):60-64.

58. Hosch T, Napolitano RE. The effect of the flake to fiber transition in silicon morphology on the tensile properties of Al-Si eutectic alloys. *Materials Science and Engineering: A*. 2010;528(1):226-232.

59. Çadırlı E, Sahin M, Turgut Y. Characterization of a directionally solidified Sn-Pb-Sb ternary eutectic alloy. *Metallography, Microstructure, and Analysis*. 2015;4(4):286-297.

60. Zhang Q, Zou H, Zhang ZF. Improving tensile and fatigue properties of Sn-58Bi/Cu solder joints through alloying substrate. *Journal of Materials Research*. 2010;25(2):303-314.